Viscoelasticity of PA/SBS/SBR Composite Modi-fied Asphalt and Asphalt Mixtures under Pressure Aging Conditions

Zongjie Yu *, Xinpeng Ling , Ze Fan , Yueming Zhou , Zhu Ma

Posted Date: 10 February 2025

doi: 10.20944/preprints202502.0577.v1

Keywords: Road Engineering; PPA/SBS/SBR Composite Modified Asphalt Mixture; FTIR; GPC; Viscoelasticity; Dynamic Modulus

Article

Viscoelasticity of PA/SBS/SBR Composite Modi-Fied Asphalt and Asphalt Mixtures under Pressure Aging Conditions

Zongjie Yu [1,2,*], Xinpeng Ling [1,2], Ze Fan [1,2], Yueming Zhou [1,2] and Zhu Ma [3]

[1] Xinjiang Institute of Transportation Sciences Co., Ltd., Urumqi, Xinjiang 830000, China

[2] Key Laboratory of Highway Engineering Technology and Transportation Industry in Arid Desert Regions, Urumqi, Xinjiang 830000, China

[3] Xinjiang Highway and Bridge Testing and Inspection Center Co., Ltd., Urumqi, Xinjiang 830000, China

* Correspondence: 13511844380@163.com

Abstract: The viscoelastic behavior of asphalt mixtures is a crucial consideration in the analysis of pavement mechanical responses and structural design. This study aims to elucidate the molecular structure and component evolution trends of PPA/SBS/SBR composite modified asphalt (CMA) under Rolling Thin Film Oven Test (RTFOT) and pressure aging (PAV) conditions, as well as to analyze the viscoelastic evolution of CMA mixtures. First, accelerated aging was conducted in the laboratory through RTFOT, along with PAV tests for 20 hours and 40 hours. Next, the microscopic characteristics of the binder at different aging stages were explored using Fourier Transform Infrared Spectroscopy (FTIR) and Gel Permeation Chromatography (GPC) tests. Additionally, fundamental rheological properties and temperature sweep tests were performed to reveal the viscoelastic evolution characteristics of CMA. Ultimately, the viscoelastic properties of CMA mixtures under dynamic loading at different aging stages were clarified. The results indicate that the incorporation of SBS and SBR increases the levels of carbonyl and sulfoxide factors while decreasing the level of long-chain factors, which slows down the rate of change of large molecule content and reduces the rate of change of LMS by over 6%, with the rate of change of overall molecular weight distribution narrowing to below 50%. The simultaneous incorporation of SBS and SBR into CMA mixtures enhances the dynamic modulus in the 25Hz and -10 ℃ range by 24.3%(AC-13), 15.4%(AC-16), and reduces the φ by 55.8%(AC-13), 40%(AC-16). This research provides a reference for the application of CMA mixtures in the repair of pavement pothole damage.

Keywords: Road Engineering; PPA/SBS/SBR Composite Modified Asphalt Mixture; FTIR; GPC; Viscoelasticity; Dynamic Modulus

1. Introduction

Asphalt aging is one of the factors leading to the deterioration of pavement performance [1]. Currently, researchers have begun to explore the effects of asphalt aging on its performance. through numerous laboratory experiments [2,3]. Studies by [4,5] have demonstrated that the complex modulus of SBS modified asphalt increases with aging time while the phase angle decreases. This trend results in reduced adhesion and the onset of stress relaxation in SBS modified asphalt. The study found that the addition of polymers can achieve three effects: first, it reduces the problem of surface raveling; second, it slows down the aging rate of the matrix asphalt; and third, it enhances the aging performance of the polymer-modified asphalt [6–9].

During the aging process of asphalt, short-chain compounds participate in addition and polymerization reactions, resulting in the formation of longer-chain compounds. The transformation of aromatic fractions and resins into asphalt contributes to the leading to asphalt hardening and embrittlement of the material [10,11]. Modified asphalt obtained by incorporating SBS and SBR into

 doi:10.20944/preprints202502.0577.v1

the base asphalt is used due to its excellent performance [12]. The presence of carbonyl compounds and sulfur oxides in aged asphalt contributes to a significant reduction in the effectiveness of SBS and SBR modifiers. Aged modified asphalt exhibits increased hardness and a notable decrease in low-temperature ductility, which reflects the combined effects of oxidation of asphalt molecules and degradation of compounds [11,13–15].

In existing research, there are numerous evaluation methods for assessing the impact of multi-field coupling effects on the performance of asphalt mixtures. Guo et al. [16] analyzed the adhesion failure patterns of asphalt mixtures under temperature-humidity coupling conditions using digital image processing technology. Yang et al. [17,18] investigated the aging characteristics of polymer-modified asphalt under temperature-irradiation coupling conditions through multi-scale morphological characterization techniques. However, the diverse evaluation methods face limitations in their promotion and application processes [19–23]. Therefore, focusing on the stress-strain response of asphalt mixtures under multi-field coupling environments and exploring the viscoelastic evolution of these mixtures can provide precise quantitative measurements of the effects of multi-field coupling [24].

Viscoelasticity is one of the essential properties that reflect the stress-strain response of materials. In the study of asphalt mixtures, dynamic and static load tests are commonly employed to evaluate the linear viscoelastic behavior of the mixtures [1]. Under dynamic loading, specimens are typically cylindrical with dimensions of Φ100 mm × h150 mm, and their performance is assessed through dynamic modulus testing. Under static loading, creep or relaxation tests are usually conducted to maintain a constant stress or strain in the asphalt mixture, characterizing its creep and stress relaxation behavior under prolonged loading or relaxation conditions. Proposed predictive methods for the viscoelastic behavior of asphalt mixtures under aging conditions through statistical analysis and the development of empirical equations [25–28]. In the conversion and analysis of viscoelasticity under dynamic and static loads extensively explored numerical methods for studying the conversion of viscoelastic properties under dynamic and static loading conditions, along with their accuracy in transformation [29–34].

GPC and FTIR are commonly used to analyze the composition and changes in asphalt. Studies have shown that polymer-modified asphalt undergoes an increase in high molecular weight molecules and a decrease in low and medium molecular weight molecules after aging. During the aging process of SBS molecules, degradation into smaller molecules also occurs [4,5,7,35,36].

In summary, while scholars have conducted extensive research on the viscoelasticity of asphalt mixtures under aging conditions, the results have varied significantly, and there is a lack of microscopic analysis on the viscoelasticity of CMA. To address this gap, this study conducted indoor aging tests on CMA mixtures using RTFOT and PAV aging protocols to obtain CMA binders and mixtures at different stages of aging. Microscopic analysis was performed using FTIR and GPC to qualitatively and quantitatively analyze the characteristic functional groups and molecular weight of CMA. Additionally, rheological performance analysis included basic performance testing and temperature scanning tests. For the viscoelastic analysis of the mixtures, dynamic modulus testing was performed under dynamic loading conditions. Through the integration of microscopic analysis, rheological performance analysis, and viscoelastic analysis, this study reveals the evolution patterns of the viscoelasticity of CMA materials under various aging conditions.

2. Materials and Methods

2.1. Aging Tests

2.1.1. RTFOT Test

The RTFOT origin is Hangzhou City, Zhejiang Province, China. The BA and CMA were placed on the aging tray, Simulate short-time thermal oxidative aging of the asphalt (163°C, 5 hours). BA is denoted as BA_{RTFOT} after the RTFOT, while CMA after the RTFOT is referred to as CMA_{RTFOT}.

 doi:10.20944/preprints202502.0577.v1

2.1.2. PAV Test

The PAV 20-hour and PAV 40-hour aging tests were carried out to simulate asphalt aging after 5-8 years and 8-12 years of service life respectively. Experimental Conditions (2.1 MPa, 100°C). BA after 20h and 40h of PAV is designated as BA_{PAV20} and BA_{PAV40}, respectively. Similarly, CMA after 20 hours and 40 hours of PAV is referred to as CMA_{PAV20} and CMA_{PAV40}, respectively.

2.2. Asphalt

This study utilized one type of base asphalt (BA) and one type of CMA, PetroChina Karamay Petrochemical Co., Ltd. 90# (Grade A) road asphalt was chosen as the BA and served as the control group. Based on prior research [12], CMA was obtained by modifying BA. The results of the main performance indicators for the two types of asphalt before and after RTFOT are presented in Figure 1.

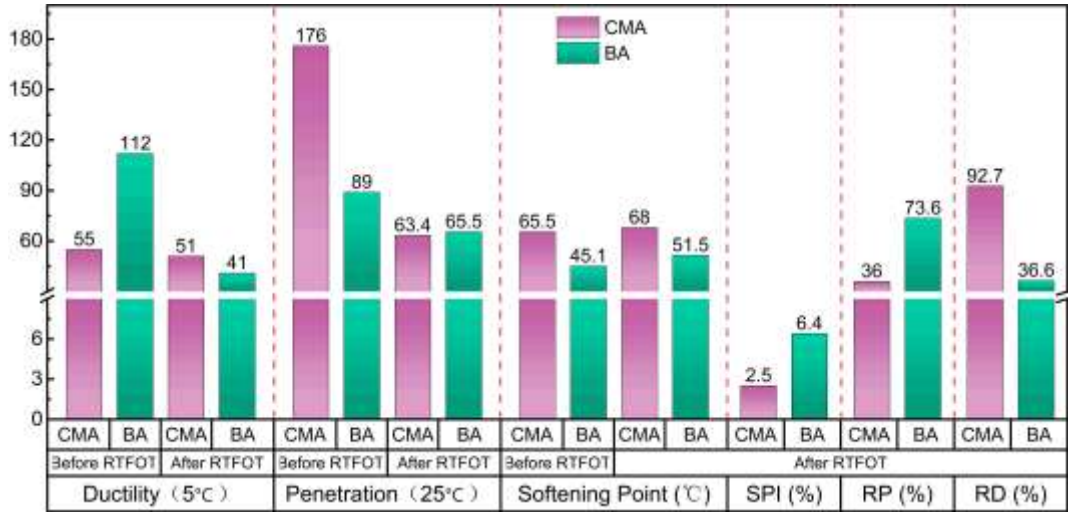

Figure 1. Main performance indexes of BA and CMA before and after RTFOT.

2.3. Dynamic Shear Rheometer (DSR) Test

DSR test were analyzed using the CV0150 AR1500ex manufactured by TA Instruments, focusing primarily on the variations in G^* and δ, as well as $G^*/\sin\delta$.

2.4. Microscopic Mechanisms

2.4.1. FTIR Test

FTIR was employed to analyze the functional groups of the binder before and after aging. The FTIR test was performed using the Nicolet iS20 Fourier Transform Infrared Spectrometer produced by Thermo Scientific in the USA. The infrared spectra wavenumber range were set as 400–4000 cm^{-1} (4 cm^{-1}, 32 scans).

2.4.2. GPC Test

Asphalt analysis was conducted using the Agilent 1260 Infinity II Gel Permeation Chromatograph and associated software manufactured by Agilent Technologies in the USA. Tetrahydrofuran (THF) was used as the mobile phase, and three chromatographic columns were connected in series to wash asphalt molecules based on their molecular sizes.

The chromatograms were divided into 13 segments and categorized into three groups: including large molecule size compounds (LMS, sections 1-5), medium molecule size compounds (MMS, sections 6-9), and small molecule size compounds (SMS, sections 9-13), and further analysis of the compositional changes of the two types of asphalt before and after aging.

 doi:10.20944/preprints202502.0577.v1

2.5. Asphalt mixture Design and Forming

Crushed stone and manufactured sand were sourced from Rongxiang Piez Stone Mine in Yanqi County, Xinjiang, China, while the mineral powder was produced by Shuo Zheng Mining Co., Ltd. in Hezhuo County, Xinjiang, China. The raw material testing results were conducted in accordance with the requirements of the "Technical Standard for Testing Aggregates in Highway Engineering" (JTG 3432-2024) and the "Technical Specifications for Construction of Asphalt Pavements" (JTG F40-2004). A summary of the test results for crushed stone, manufactured sand, and mineral powder is presented in Table 1.

Table 1. Test results of crushed stone, machine-made sand and mineral powder.

Detecting parameter / sample name	Apparent relative density	Relative density of gross volume	Water absorption (%)	detection result
Gravel (15-20) mm	2.871	2.842	0.28	Qualified
Gravel (10-15) mm	2.862	2.827	0.43	
Gravel (5-10) mm	2.855	2.803	0.64	
Gravel (3-5) mm	2.849	2.794	0.69	
Machine sand (0-3) mm	2.821	2.755	/	
Mineral powder	2.718	/	/	
Technical requirements	Gravel≮2.60 Machine sand≮2.50	/	≯2.0	/

The asphalt mixture proportions included two types of asphalt (BA 、CMA) and two gradations (AC-13、AC-16). The road performance of the CMA mixture was evaluated through water stability tests, rutting tests, and low-temperature cracking resistance tests, and subsequently compared with that of the BA mixture. Two types of BA mixtures is denoted as BA_{AC-13} andBA_{AC-16}, while CMA is referred to as CMA_{AC-13} and CMA_{AC-16}.

The asphalt mixture was initially formed using a rotary compactor to achieve, The specimen specification (Φ150 mm × h170 mm). After demolding, the mixture was placed at room temperature for 48 hours, then cored and cut into specimens (Φ100 mm × h150 mm).

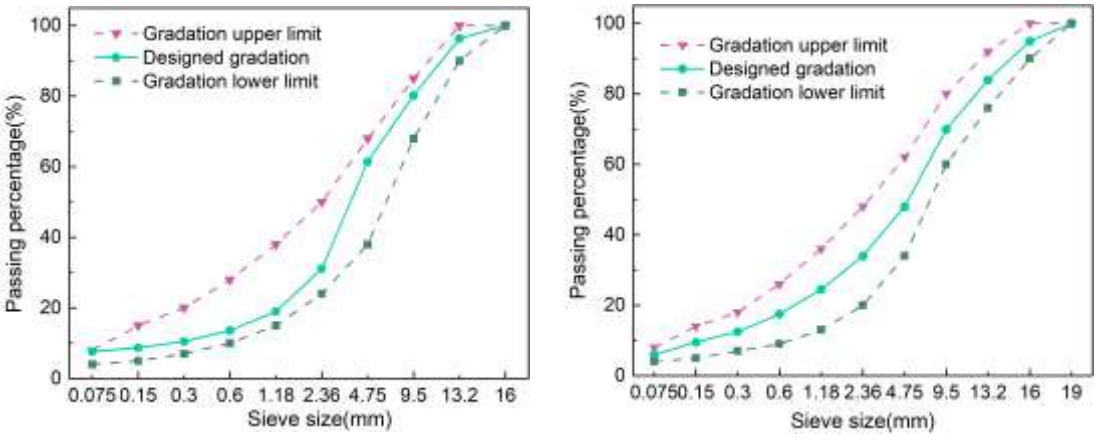

(**a**) (**b**)

Figure 2. The designed gradation curves: (**a**) AC-13; (**b**) AC-13.

2.6 Asphalt Mixture Viscoelasticity Test

The viscoelastic properties of the CMA mixture were tested using a UTM-130 testing machine. The dynamic modulus test was employed to characterize the viscoelastic behavior. Five experimental temperatures were used: (-10, 4.4, 21.1, 37.8, and 54.4)℃, Six loading frequencies were used: (0.1, 0.5,

 doi:10.20944/preprints202502.0577.v1

1, 5, 10, and 25) Hz [31,36]. Additionally, the dynamic modulus test is a non-destructive testing method.

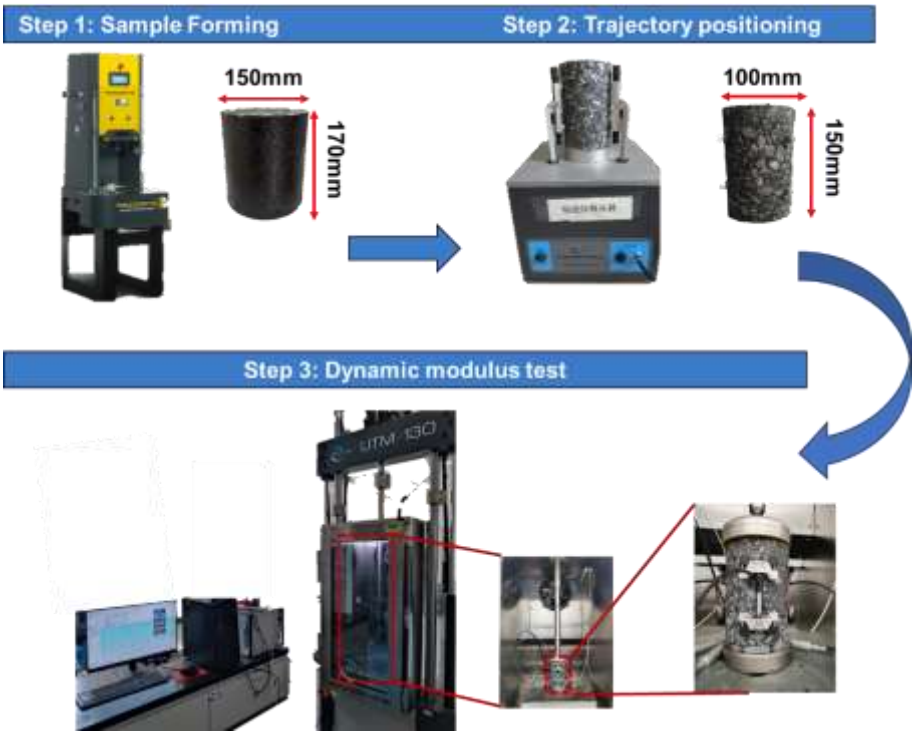

Figure 3. Dynamic modulus test

3. Results

3.1. Test results of Asphalt Rheological Properties

The complex modulus (G^*) represents the capability of a material to resist shear deformation, while the phase angle (δ) signify the ratio of viscous (non-recoverable) to elastic (recoverable) components. The G^* aging index C_{MAI} and δ aging index P_{AAI} were used to evaluate the aging degree of the two types of asphalt. A higher C_{MAI} and a lower P_{AAI} indicate more severe aging. The calculations for C_{MAI} and P_{AAI} are as follows:

$$C_{MAI} = G^{*1} / G^{*2}, \quad (1)$$

$$P_{AAI} = \delta_1 / \delta_2, \quad (2)$$

Equation: G^{*1}, G^{*2}: G^* before and after aging; δ_1, δ_1: δ before and after aging.

Figure 4 (a), (b), (c) depict the G^*, δ, and $G^*/\sin\delta$ of BA and CMA before and after aging. It can be observed from Figure 4 (a), (b), (c) that the G^* of both asphalt samples decreases with increasing temperature. Contrastingly, the G^* values of both asphalt samples significantly increased after RTFOT aging compared to the unaged samples, with CMA showing a more pronounced increase in G^* values than BA. Following RTFOT aging, the δ curves of the two asphalt samples exhibited distinct trends. A reduction in δ signifies a decrease in the ratio of viscous to elastic components, indicating an increase in the stiffness of the asphalt. Post-RTFOT aging, BA demonstrated a higher δ compared to CMA

 doi:10.20944/preprints202502.0577.v1

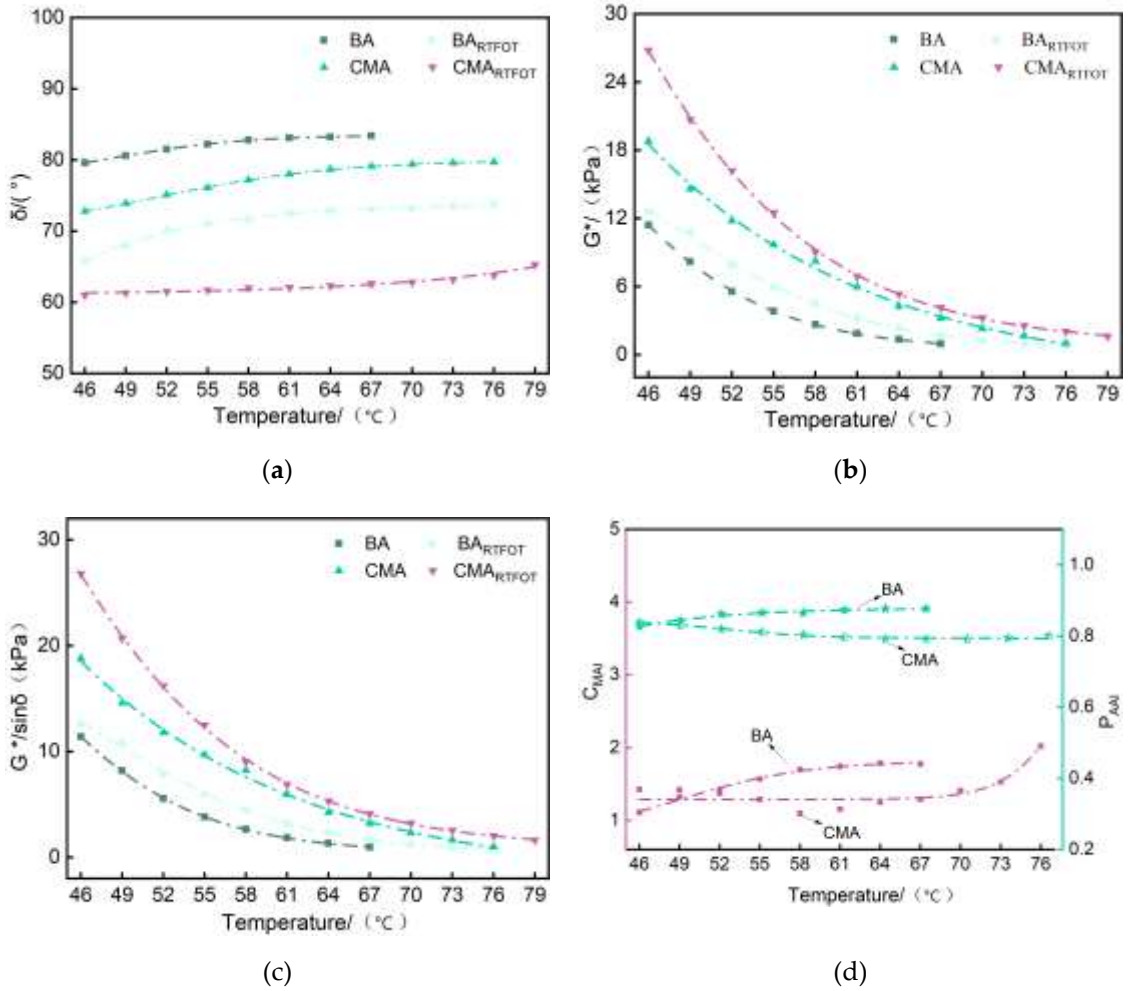

Figure 4. Rheological properties before and after RTFOT aging of BA and CMA. **(a)** δ; **(b)** G^*; **(c)** $G^*/\sin\delta$; **(d)** C_{MAI} and P_{AAI}.

Figure 4 (d) displays the changes in C_{MAI} and P_{AAI} for BA and CMA before and after aging. It is evident from Figure 4 (d) that at the same testing temperature, CMA exhibited lower values within the range of 46–76 °C. After RTFOT aging, the BA C_{MAI} ranged between 1.1 and 1.8, while CMA ranged between 1.1 and 2.0, with a more pronounced difference post-RTFOT aging. The trend for BA showed an initial increase followed by stabilization in C_{MAI} with temperature variation. However, CMA followed by an increase after 46 °C, indicating its superior aging resistance at high temperatures.

Figure 4 (d) illustrates the changes in P_{AAI} for BA and CMA before and after aging. It is evident from Figure 4 (d) that BA overall exhibited lower P_{AAI} values compared to CMA. Post-RTFOT aging, the P_{AAI} values of BA slightly increased with temperature, whereas the P_{AAI} values of CMA post-RTFOT aging did not strictly increase with temperature and showed a slight decrease within the 46–64°C range, followed by a slight increase within the 64–76°C range.

Based on the observed changes in G^* and δ, it was determined that the degree of hardening for both asphalt types was greater following RTFOT aging than prior to aging. Both types of asphalt demonstrated strong long-term aging resistance, with CMA exhibiting superior aging resistance at elevated temperatures compared to BA. This observation is consistent with previous studies that suggest polymer-modified additives improve aging resistance.

3.2 Microscopic Characteristic Analysis

To investigate the changes in viscoelastic properties of the two types of asphalt at the molecular structure level, FTIR spectroscopy was employed for quantitative analysis of the carbonyl index ($I_{c=o}$),

 doi:10.20944/preprints202502.0577.v1

sulfoxide index ($I_{s=o}$), long-chain index (I_{LC}), branched index (I_{BC}), aromatic index (I_{ar}), and aliphatic index (I_{al}) during the aging process of the asphalt. The $I_{c=o}$ and $I_{s=o}$ indices were used to characterize the degree of aging of the asphalt, while the variations in I_{LC}, I_{BC}, I_{ar}, and I_{al} were attributed to the evolution of the viscoelastic properties of the asphalt.

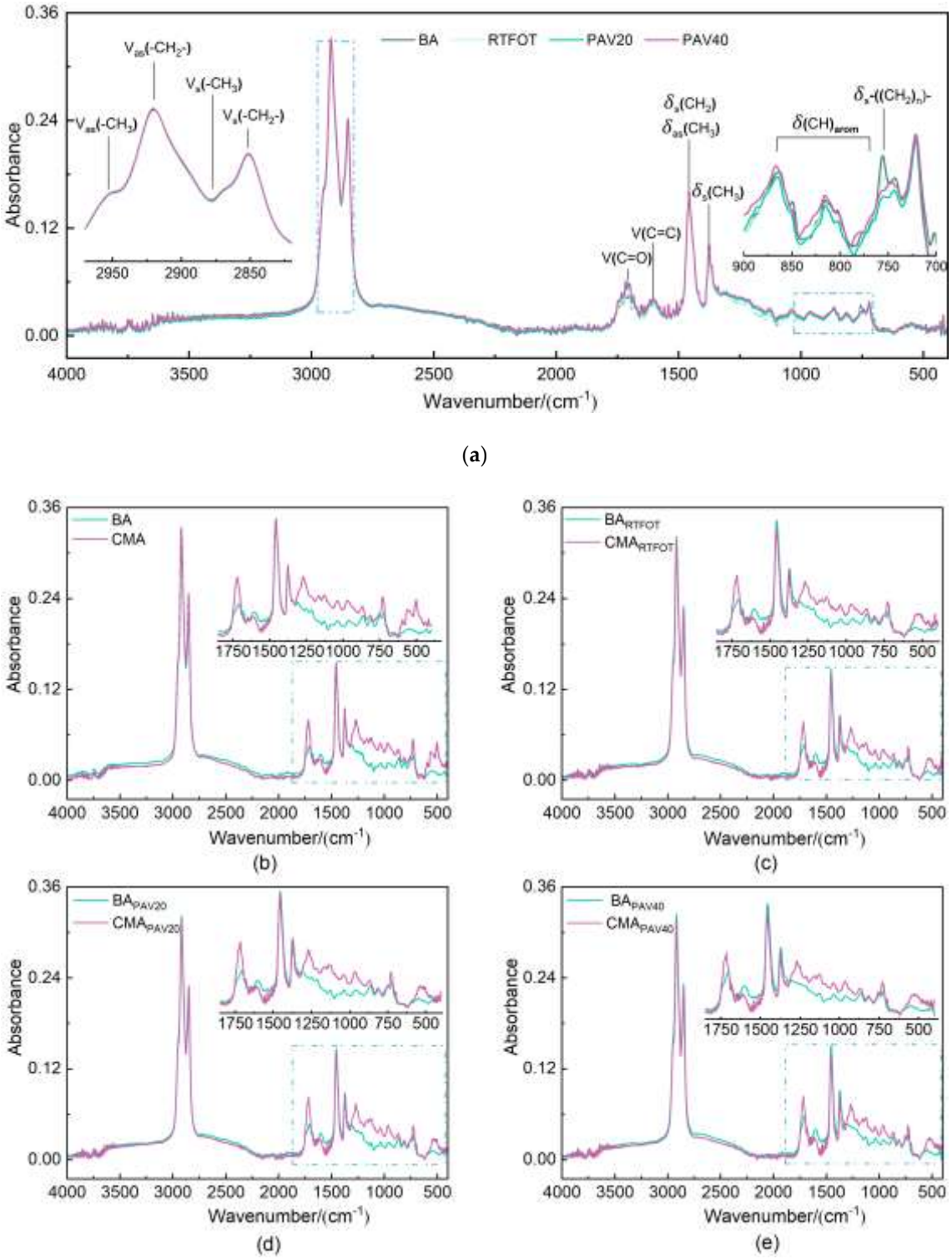

Figure 5. FT-IR spectra of BA and CMA with different aging conditions. **(a)** FTIR spectra of BA and CMA with different aging conditions; **(b)** BA and CMA; **(c)** RTFOT; **(d)** PAV20; **(e)** PAV40.

 doi:10.20944/preprints202502.0577.v1

Figure 6 illustrates the trend of changes in the $I_{c=o}$ and $I_{s=o}$ as a function of aging degree. During the aging process, carbon oxidation occurs in the carbon atoms of the aromatic rings near the side chains, resulting in the formation of $I_{C=O}$, while the sulfur present in the asphalt undergoes oxidation to generate $I_{c=o}$. As the aging time increases, the oxidation reactions in the asphalt become more pronounced, leading to higher concentrations of $I_{c=o}$ and $I_{s=o}$. The test results and analyses presented in Figure 6 are consistent with these findings. Furthermore, the variations in $I_{c=o}$ and $I_{s=o}$ for the binders modified with SBS and SBR show a trend of initially decreasing followed by increasing, indicating a certain degree of mitigation of the aging process of the binder. This may be attributed to the absorption of lighter components by the SBS and SBR, indirectly slowing down the aging of the constituents within the asphalt. Additionally, SBS and SBR can gradually release these lighter components during the aging process, compensating for the components lost due to aging. The polymer chains in SBS and SBR also act to obstruct oxygen penetration into the asphalt, thereby reducing the rate of aging [37].

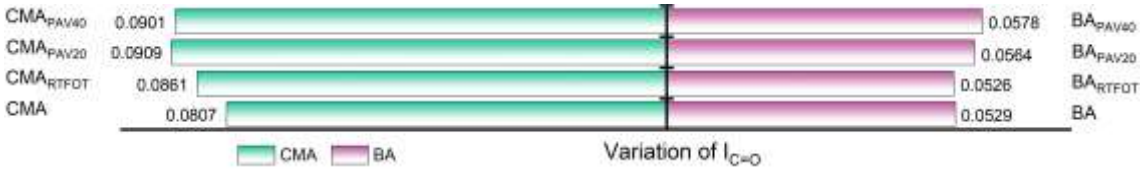

(**a**)

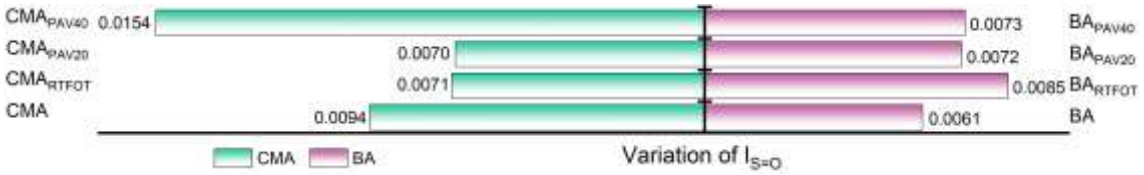

(**b**)

Figure 6. Changes in functional group indicators: **(a)** Variation of $I_{C=O}$; **(b)** Variation of $I_{S=O}$.

In addition to the formation of $I_{s=o}$ and $I_{c=o}$, the aging process of asphalt is accompanied by condensation and addition reactions, wherein small molecules aggregate to form larger molecules. This leads to a reduction in the number of branched chains, resulting in longer molecular chains and an increased proportion of long chains. Figure 8 illustrates the trends of changes in the I_{LC} and I_{BC} during the aging process. With increasing aging severity, I_{LC} rises while I_{BC} decreases. For I_{LC}, the incorporation of SBS and SBR has a mitigating effect on its increase, indicating that the addition of SBS and SBR can effectively reduce the polymerization of long chains during the aging process. Conversely, the incorporation of SBS and SBR also slows down the reduction in I_{BC}, leading to an overall shortening of the asphalt molecular chains. As a result, the asphalt molecules with SBS and SBR additives exhibit greater flexibility compared to those without these modifiers.

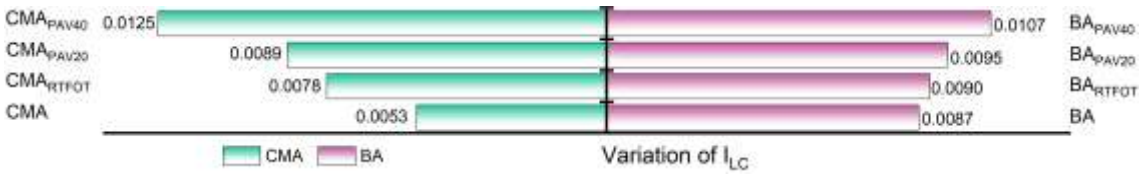

(**a**)

 doi:10.20944/preprints202502.0577.v1

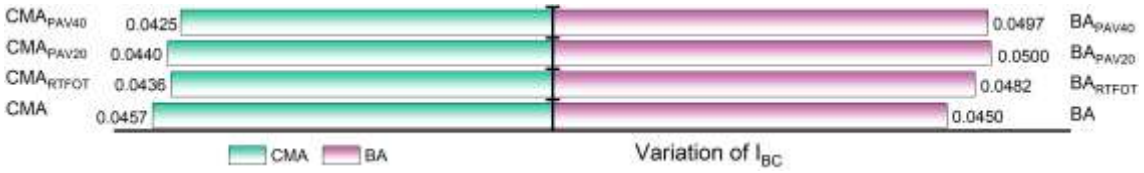

(**b**)

Figure 7. Changes in functional group indicators: **(a)** Variation of I_{LC}; **(b)** Variation of I_{BC}.

During the aging process, the aliphatic components in asphalt gradually convert to aromatic compounds, resulting in a decrease in aliphatic content and an increase in aromatic content, as shown in Figure 8. The aromatic formation can be demonstrated as a combined result of two processes: the full hydrogenation of aromatic rings and the alkyl substitution of cycloalkanes. Notably, the incorporation of SBS and SBR slows the rate of reduction of aliphatic molecules during aging, thereby mitigating the aromatic conversion compared to binders without these additives. This indicates that during thermal oxidative aging, the absorption of lighter components by SBS and SBR effectively slows down part of the aromatic conversion process of aliphatic molecules. Furthermore, the long polymer chains of SBS and SBR provide effective barriers against the further penetration of oxygen, thereby reducing the conversion of aliphatic to aromatic compounds [37,38].

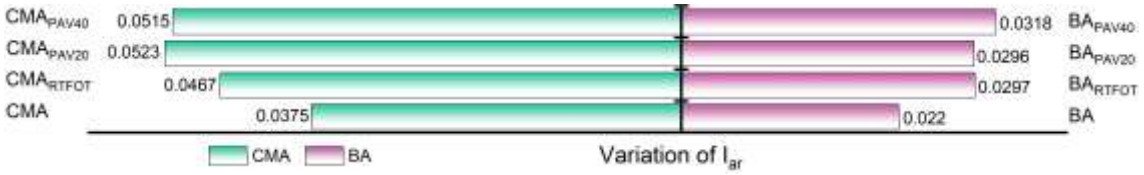

(**a**)

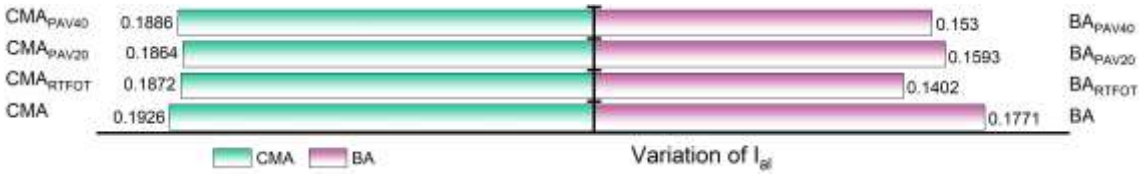

(**b**)

Figure 8. Changes in functional group indicators: **(a)** Variation of I_{ar}; **(b)** Variation of I_{al}.

Figure 9 illustrates the trends in changes of $I_{c=o}$, $I_{s=o}$, I_{LC}, I_{BC}, I_{ar}, and I_{al} before and after aging. The I_{ar} of BA decreased by 13.6%, while the I_{ar} of CMA also decreased by 2%. Additionally, the I_{BC} of CMA decreased by 6.9%. The growth rates of the other parameters for both BA and CMA before and after aging exceeded 9.3%, with CMA displaying a remarkable increase of 136% in I_{LC}.

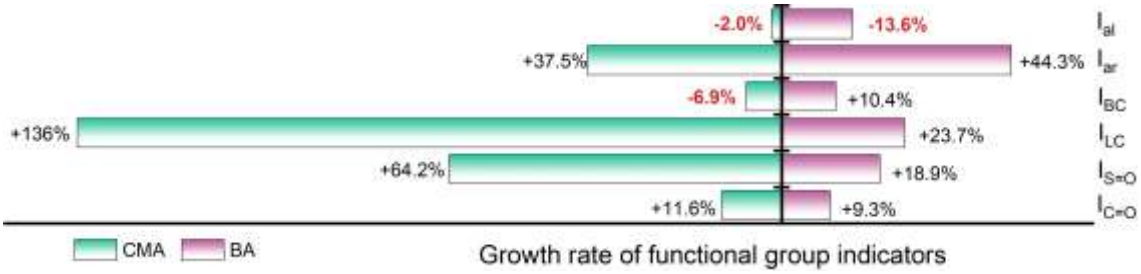

Figure 9. Changes in functional group indicators at different aging stages.

3.3 GPC Analysis

 doi:10.20944/preprints202502.0577.v1

By using GPC, the changes in number-average molecular weight (M_n), weight-average molecular weight (M_w), and polydispersity index (PDI) of BA and CMA samples before and after aging with RTFOT, PAV20, and PAV40 are obtained and depicted in the curve shown in Figure 11. Studies have shown that M_w is sensitive to compounds with high molecular weights; a higher M_w indicates a higher amount of high-molecular-weight substances. On the other hand, M_n is sensitive to compounds with low molecular weights; a larger M_n indicates a higher amount of low-molecular-weight substances. The polydispersity coefficient PDI represents the distribution of both high and low-molecular-weight substances, with a larger PDI indicating a more dispersed distribution of all molecules [39–41].

Figure 10 (a) and (c) show the M_w distribution of BA and CMA during the aging process. The x-axis represents the logarithmic weight-average molecular weight of asphalt, while the y-axis represents the relative content of asphalt. Figure 10(a) and (c) demonstrate that after RTFOT aging, PAV20 aging, and PAV40 aging, the overall molecular weight of asphalt shifted towards larger molecules. During aging, the lighter components in asphalt volatilize and transform into colloids and asphaltenes. Aging ultimately leads to a decrease in the content of lighter components in asphalt and an increase in the content of asphaltenes. Asphaltenes are high-molecular-weight substances. Consequently, after aging, the molecular weight distribution curve of asphalt gradually shifts to the right, indicating a reduction in polymer molecular weight due to the degradation of long-chain polymers [42].

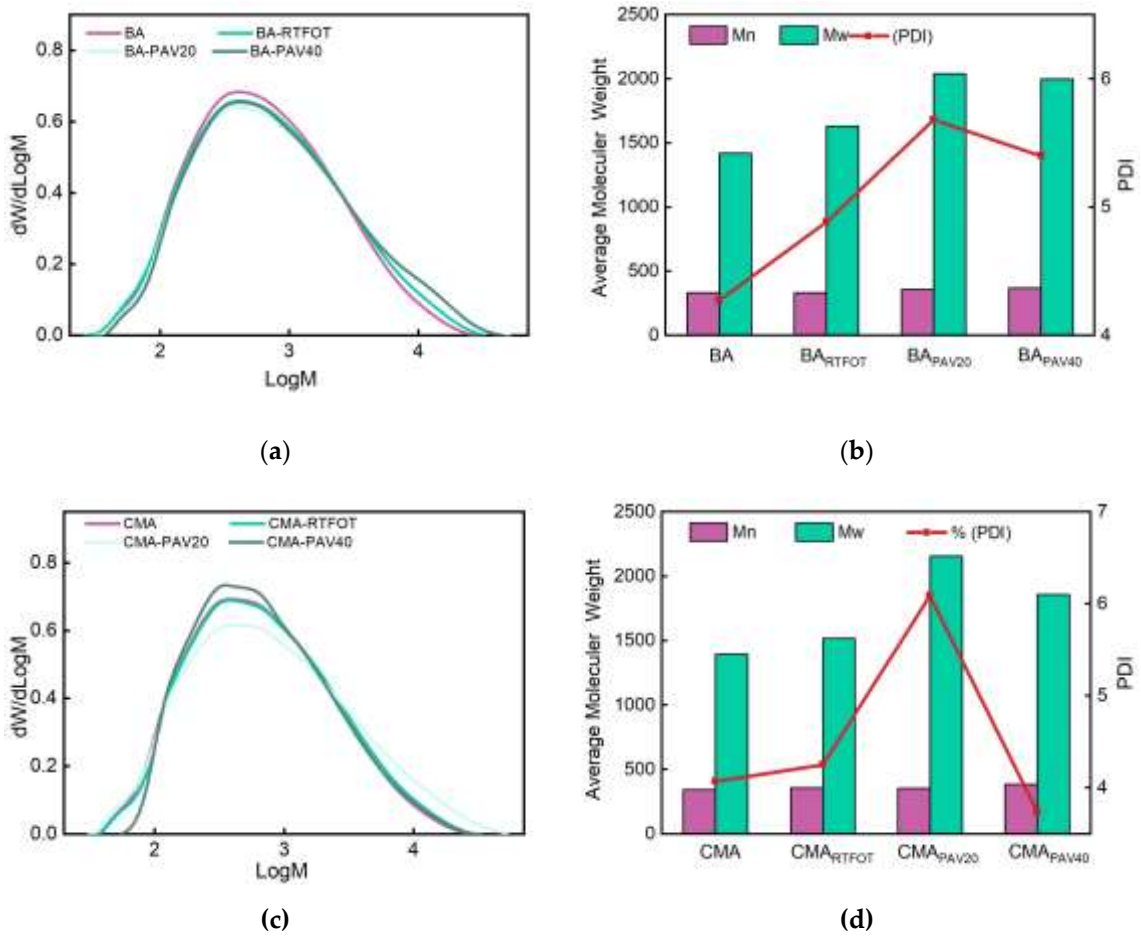

Figure 10. GPC results of BA and CMA: **(a)** M_w distribution of BA; **(b)** M_w of BA of different aging conditions; **(c)** M_w distribution of CMA; **(d)** M_w of CMA of different aging conditions.

 doi:10.20944/preprints202502.0577.v1

Figures 10 (b) and (d) reveal that after RTFOT aging and PAV20 aging, BA and CMA show varying degrees of increase in M_n, M_w, and PDI values, indicating an increase in molecular weight and dispersity of aged asphalt. This indicates a reduction in low M_w components and an increase in high M_w components following RTFOT and PAV20 aging, which enhances the shear resistance of aged asphalt and improves its high-temperature performance. The polydispersity coefficient PDI increases for both asphalt types after RTFOT aging and PAV20 aging, indicating a more dispersed molecular distribution after these aging processes. However, after PAV40 aging, the M_n, M_w, and PDI values of BA and CMA show varying degrees of decrease, mainly due to degradation of long-chain polymers during the aging process [39].

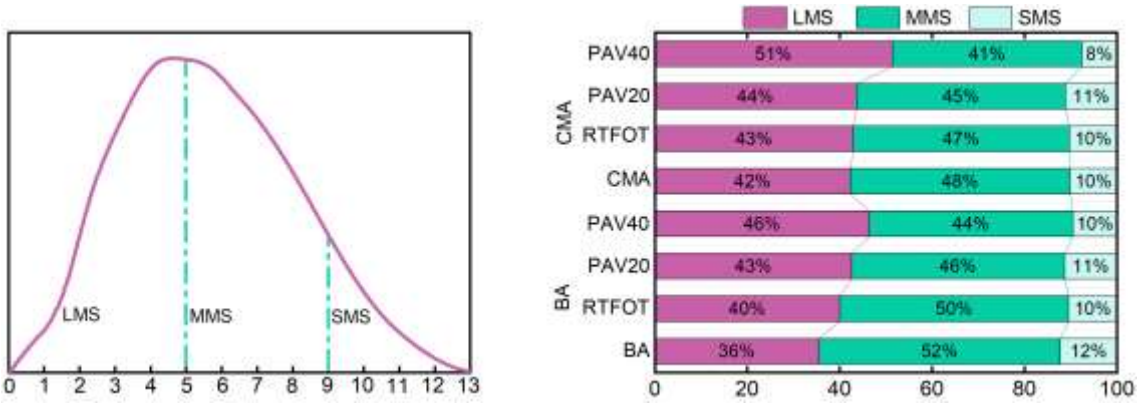

(**a**) (**b**)

Figure 11. Changes in molecular weight of BA and CMA before and after aging: **(a)** Division of LMS, MMS, and SMS; **(b)** Molecular weight distribution results.

Figure 11 shown that before aging, the content of LMS in base asphalt is 36%, MMS content is 52%, and SMS content is 12%. The content of LMS, MMS, and SMS in CMA is 42%, 48%, and 10%, respectively. During the aging process, both types of asphalt show a decrease in MMS and SMS content, with an increase in LMS content. This is due to oxidation reactions during aging, leading to the conversion of non-polar components into polar components, as well as the evaporation of SMS at high temperatures, resulting in a reduction of lower molecular weight components in the asphalt [4,43,44]. This is corroborated by the analysis in Figure 11. After RTFOT aging, the content of LMS, MMS, and SMS in base asphalt is 40%, 50%, and 10%, respectively, while for CMA it is 43%, 47%, and 10%. Following PAV20 aging, the content of LMS, MMS, and SMS in BA is 43%, 46%, and 11%, and for CMA it is 44%, 45%, and 11%. After PAV40 aging, the content of LMS, MMS, and SMS in BA is 46%, 44%, and 10%, and in CMA it is 51%, 41%, and 8%. The molecular weight of base asphalt and CMA increases after RTFOT aging and PAV aging. This indicates that the aging level of asphalt is significantly more severe after PAV aging than RTFOT aging, and CMA exhibits superior resistance to long-term hot oxygen aging. The decrease in peak values of the SBS+SBR molecular curve after aging suggests a reduction in the number of SBS+SBR molecules after aging, indicating that the SBS+SBR molecules have already played a role and delayed the aging process of modified asphalt, resulting in an overall increase in asphalt molecular mass [43]. The changes in asphalt molecular weight lead to an increase in the complex modulus of asphalt at the macro level, consistent with the changes in rheological properties of aged asphalt in this experiment [2].

The aforementioned study reveals that after aging, the number of high-molecular-weight molecules increases in CMA, while the number of low and medium-molecular-weight molecules decreases [2–4,43].

Preprints.org (www.preprints.org) | NOT PEER-REVIEWED | Posted: 10 February 2025 doi:10.20944/preprints202502.0577.v1

3.4. High and Low Temperature Performance of Asphalt Mixture

3.4.1. Marshall Test

The Marshall test results for the optimal asphalt-to-aggregate ratios of the BA_{AC-13}, BA_{AC-16}, CMA_{AC-13}, and CMA_{AC-16} asphalt mixtures are presented in Figure 12.

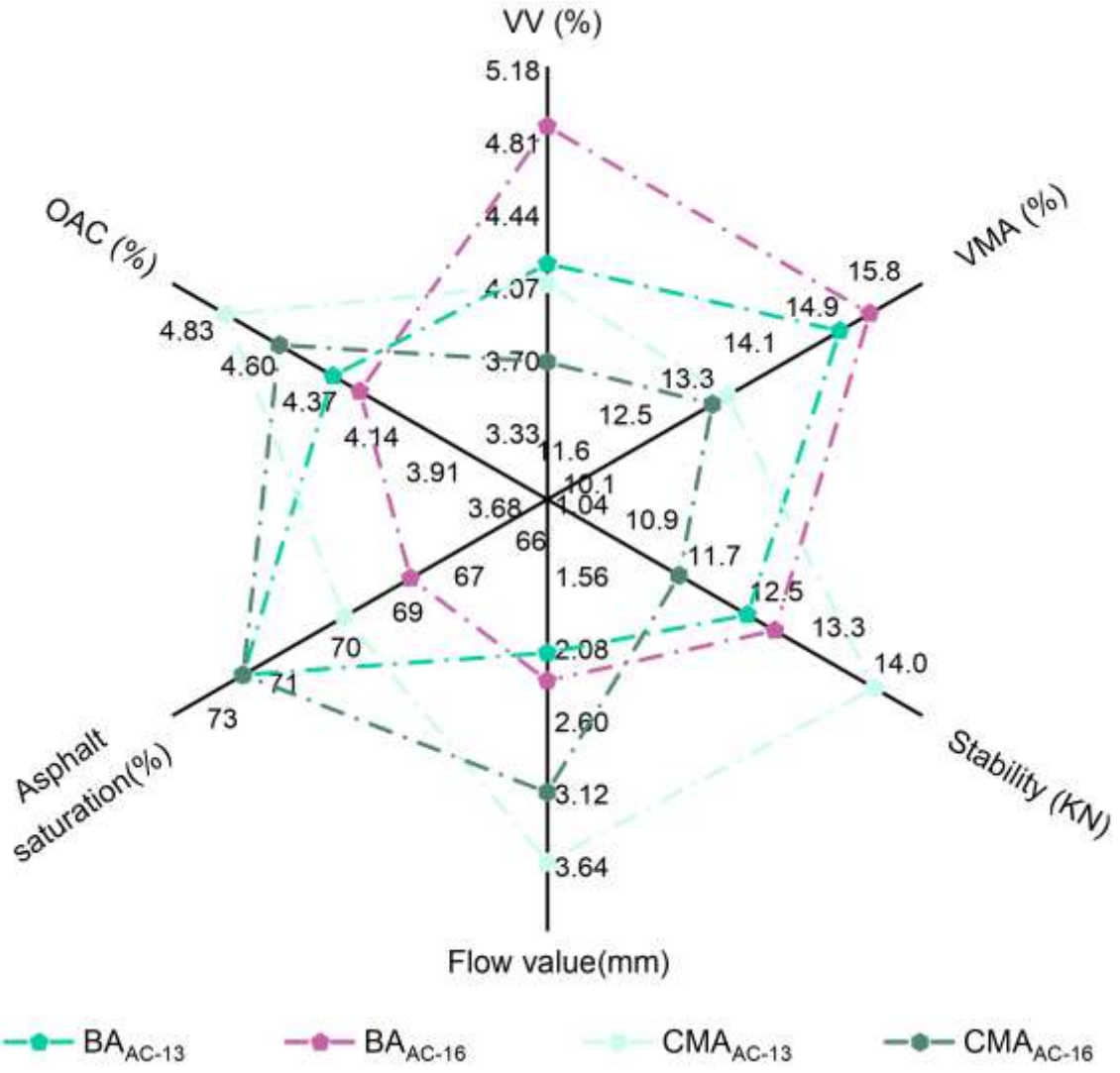

Figure 12. Marshall test results.

As shown in Figure 12, the incorporation of SBS and SBR increased the stability value of the BA mixture. As previously mentioned, this is attributed to the addition of polymers, which enhances the adhesion of BA, thereby reducing the stability values [33–35] and increasing the maximum load that the CMA mixture can bear, which is reflected in the stability value. Additionally, an increase in asphalt content may lead to a higher proportion of free asphalt, which could also decrease the Marshall stability value of the asphalt mixture.

3.4.2. Analysis of Road Performance

A comparative performance analysis was conducted between the CMA mixture and the BA mixture, focusing on their high-temperature stability(Dynamic stability(DS)), low-temperature cracking resistance (Bending tensile strength (R_B); Maximum bending tensile strain (ε_B); Flexural stiffness modulus (S_B)), and water stability(Residual stability(M_{S0}); Freeze-thaw splitting strength ratio (TSR)), among other road performance characteristics.

 doi:10.20944/preprints202502.0577.v1

Figure 13 presents the results of road performance tests for four types of asphalt mixtures. The DS values for the four mixtures are 1135, 1055, 3365, and 3172 times/mm, all of which meet the highest requirements specified in the JTGE20-2011 standard, namely, greater than 800 times and 2800 times/mm. The results indicate that the polymer network crosslinking structure inherent in the CMA system enhances the stiffness and high-temperature stability of the CMA mixture, resulting in excellent high-temperature rutting resistance.

The R_B of $\mathrm{CMA_{AC-16}}$ is 1.3 times that of $\mathrm{BA_{AC-16}}$. Additionally, the ε_B for the four asphalt mixtures is ranked from smallest to largest as follows: $\mathrm{BA_{AC-13}} < \mathrm{BA_{AC-16}} < \mathrm{CMA_{AC-13}} < \mathrm{CMA_{AC-16}}$. The results indicate that the low-temperature cracking resistance of the CMA mixtures is superior to that of the BA mixtures. The incorporation of SBS and SBR has improved the low-temperature performance of the CMA mixtures, achieving an enhancement of 133% compared to the BA mixtures, thereby meeting the highest requirement specified in the standards, which is greater than 2800.

The M_{S0} and the TSR for all four asphalt mixtures meet the standard's highest requirements, specifically, residual stability greater than 85% and a TSR greater than 80%. The M_{S0} value for $\mathrm{CMA_{AC-16}}$ is notably higher, exceeding that of $\mathrm{BA_{AC-16}}$ by 10%. Furthermore, a comparison of TSR indicates that the M_{S0} of CMA asphalt mixtures is significantly greater than 10% in the BA mixtures. These results demonstrate that CMA mixtures exhibit excellent water stability, and the addition of SBS and SBR significantly enhances the adhesion and aggregate coating performance of CMA. This, in turn, reduces the susceptibility of the modified CMA asphalt system to moisture and improves the resistance of the CMA mixtures to water damage and frost.

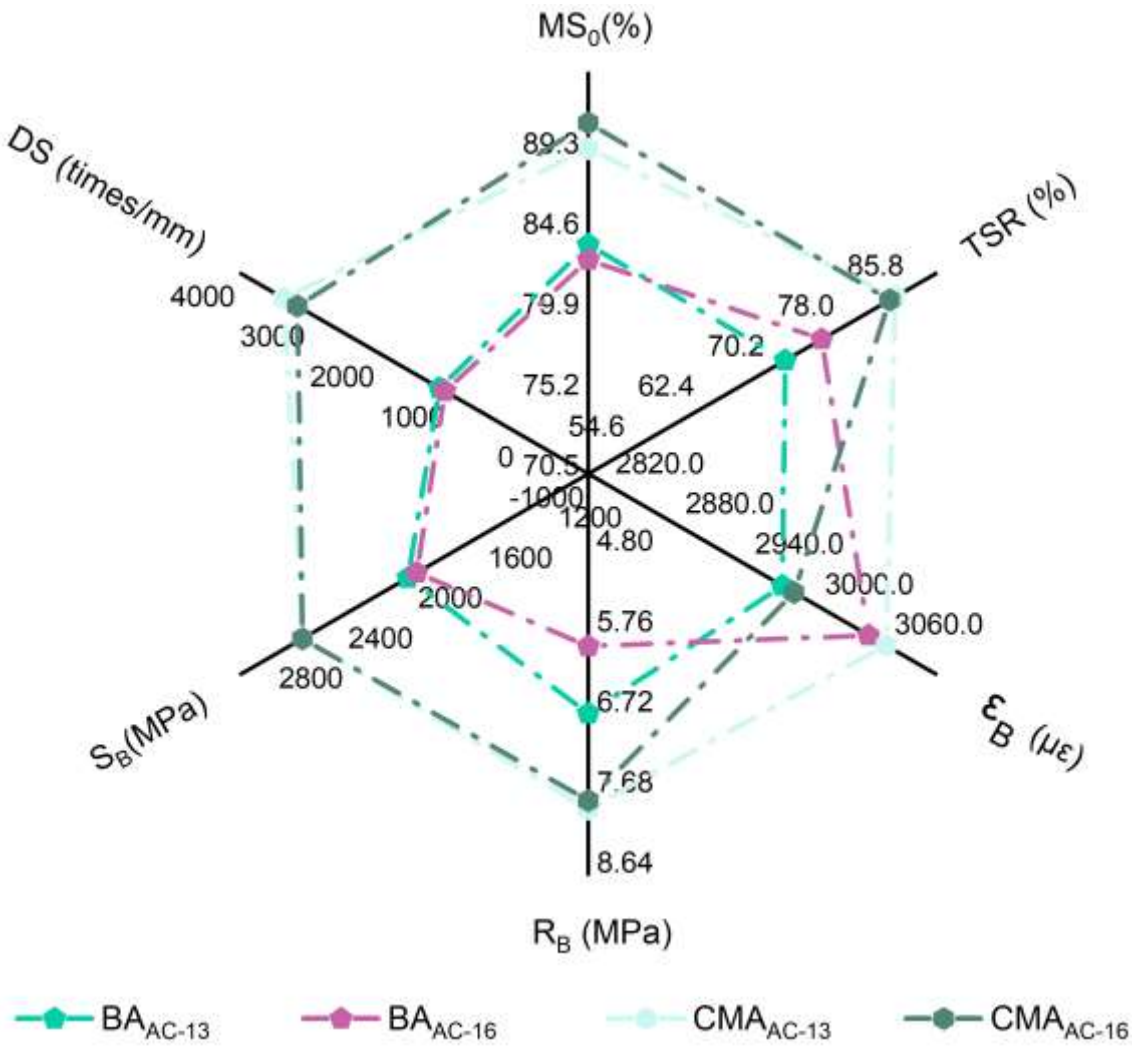

 doi:10.20944/preprints202502.0577.v1

Figure 13. Results of the Analysis of Road Performance Indicators.

3.5 Viscoelasticity

For the dynamic modulus (E^*) of the four types of asphalt mixtures, an improved Sigmoid model was used to establish the master curve of E^* at the reference temperature [26,30]. The Sigmoidal model is expressed as follows in Equation (3):

$$lg|E^*| = \varphi + \alpha/\left(1 + e^{\beta+(\gamma lgf_r)}\right) \quad (3)$$

Equation: $|E^*|$ is the dynamic modulus, MPa; φ is the logarithm of the minimum value of the E^*; α is the logarithm of the difference between the maximum and minimum E^* values; β and γ are parameters describing the shape of the master curve. The lgf_r as shown in Equation (4):

$$lgf_r = lgf + lg\alpha_T \quad (4)$$

Equation: lgf_r is the reduced frequency at the reference temperature, Hz; $lg\alpha_T$ is the shift factor, a function of temperature T; and f is the frequency, Hz.

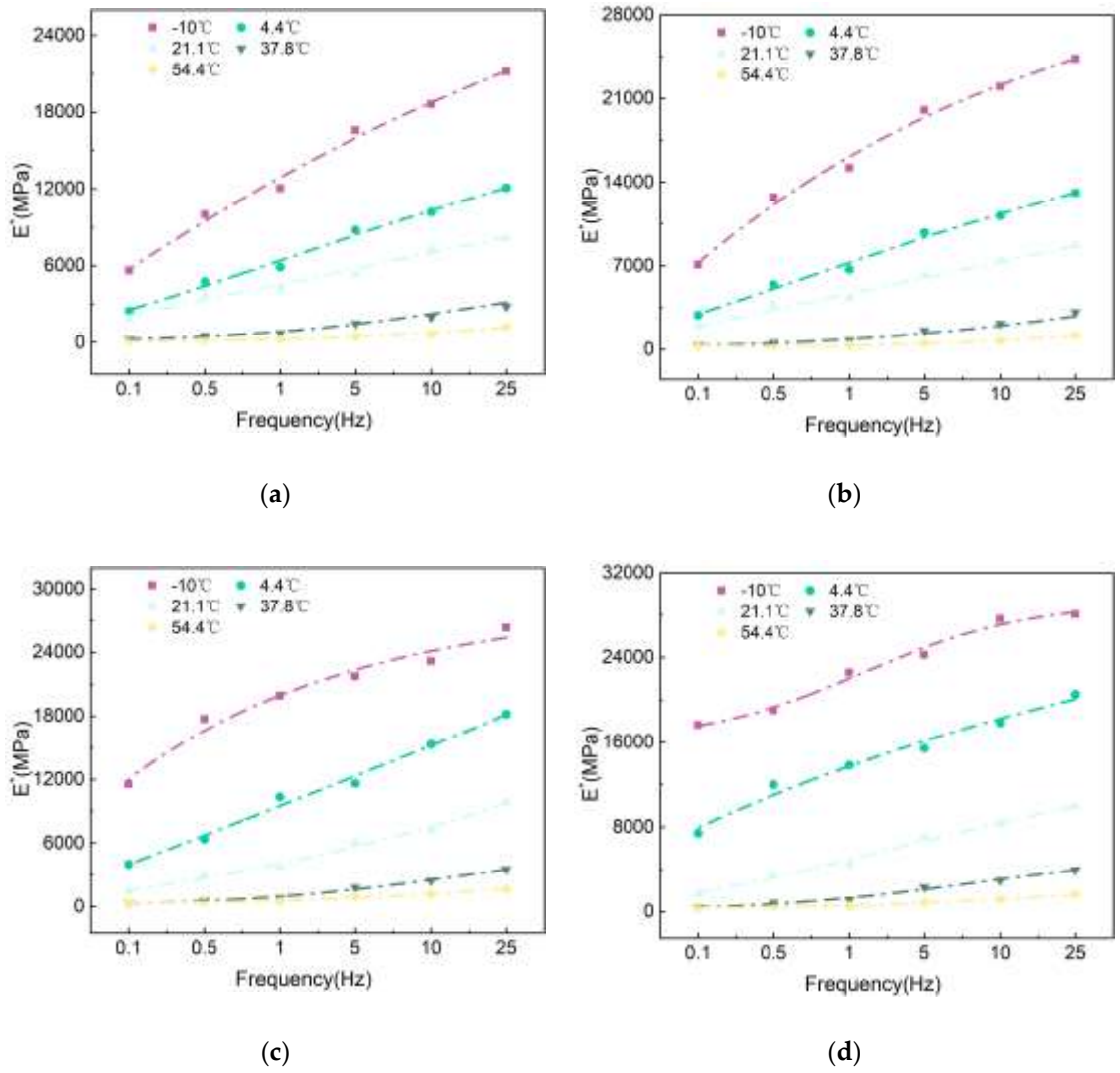

Figure 14. E^*: **(a)** BA_{AC-13}; **(b)** BA_{AC-16}; **(c)** CMA_{AC-13}; **(d)** CMA_{AC-16}.

Figures 14 and 15 show that the E^* of asphalt mixtures gradually increase with frequency at the same temperature, while at the same frequency, the E^* decreases as temperature rises. As the temperature increases, the elasticity of the asphalt mixture weakens, and its viscosity enhances,

 doi:10.20944/preprints202502.0577.v1

causing the material properties to lean more towards viscous behavior. Consequently, the E^* of the asphalt mixture decreases, making it less capable of resisting permanent deformation. Under dynamic loading conditions, the simultaneous incorporation of SBS and SBR into CMA mixtures increases the dynamic modulus in the 25Hz and -10 ℃ range by 24.3%(AC-13), 15.4%(AC-16), and reduces the φ by 55.8%(AC-13), 40%(AC-16).

Taking CMA_{AC-16} as an example, the variation of E^* with temperature exhibits a significant nonlinear characteristic. Taking 0.5 Hz as an example, the E^* value at 54.4 °C is only 8.6% of that at 21.1 °C. As the temperature increases (or the frequency decreases), the asphalt mixture softens and approaches a more viscous state, resulting in a decrease in E^* and an increase in the phase angle δ. Under high-temperature conditions (or low-frequency conditions), the influence of asphalt on the mixture diminishes; at this point, the primary factor driving the modulus variation of the asphalt mixture is the interlocking force of the aggregates. Further increases in temperature (or reductions in frequency) lead to a decrease in φ, as well as a reduction in E^*, although the values begin to stabilize.

At the same temperature and frequency, the E^* of BA is lower than that of CMA, and the change rate of the E^* of the CMA mixture in response to temperature is smaller than that of BA. In the low-frequency range of 0.1 Hz to 1 Hz, there is a significant increase in the E^* values; however, this increase becomes more gradual between 1 Hz and 25 Hz. This is mainly because, at higher loading frequencies, the asphalt pavement approaches elastic deformation, preventing further increases in the E^*. Between -10 °C and 21.1 °C, the E^* of the asphalt mixture decreases rapidly, indicating that the E^* is considerably affected by temperature in the low-temperature range, while the impact diminishes after 21.1 °C.

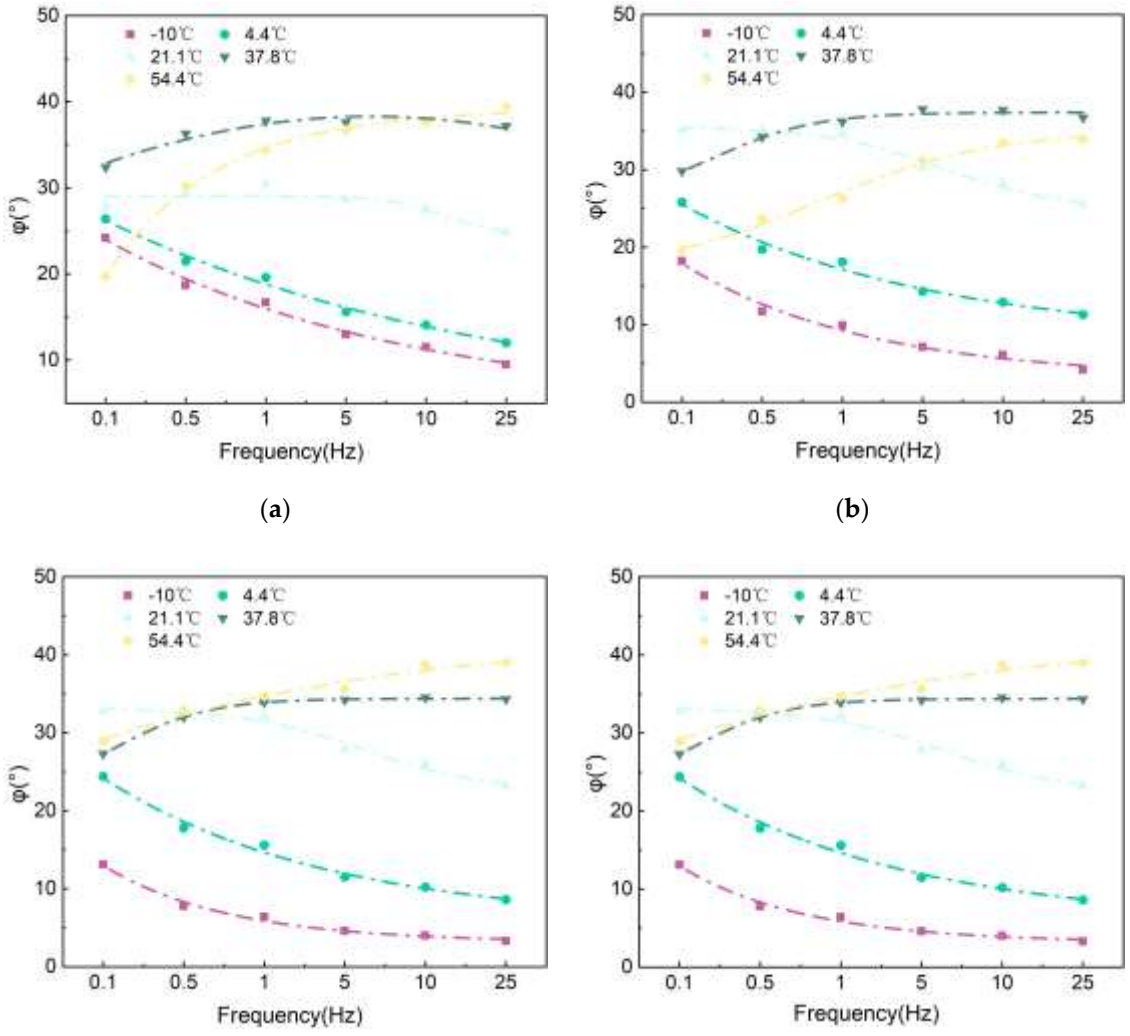

(**a**) (**b**)

 doi:10.20944/preprints202502.0577.v1

(**c**) (**d**)

Figure 15. φ: **(a)** BA_{AC-13}; **(b)** BA_{AC-16}; **(c)** CMA_{AC-13}; **(d)** CMA_{AC-16}.

Analyzing the variation of E^* with temperature (frequency) reveals that at higher temperatures (or lower frequencies), the E^* value decreases and approaches the minimum value E^*_{min}. Conversely, at lower temperatures (or higher frequencies), the E^* value increases and approaches the maximum value E^*_{max}. The generalized logarithmic Sigmoidal model effectively captures the variation characteristics of E^*.

The Sigmoid model demonstrates a good fitting performance, with an average coefficient of determination (R^2) exceeding 0.9445. Figures 14, 15, and 16 illustrate the E^*, φ, and master curve of E^*. As the test frequency decreases, the phase angle initially increases and then decreases, indicating the presence of an inflection point in the master curve. This behavior is attributed to the greater viscosity of the binder at low frequencies and high temperatures, where the aggregate skeleton responds to external stress and strain. As the test frequency gradually increases, the binder exhibits more elastic behavior under low-temperature and high-frequency conditions, leading to a gradual decrease in phase angle and an increase in dynamic modulus. The generalized logarithmic Sigmoidal model can be utilized to compute the master curve of dynamic viscoelastic parameters for the CMA mixture, enabling a comprehensive expression of the dynamic mechanical characteristics of the CMA mixture.

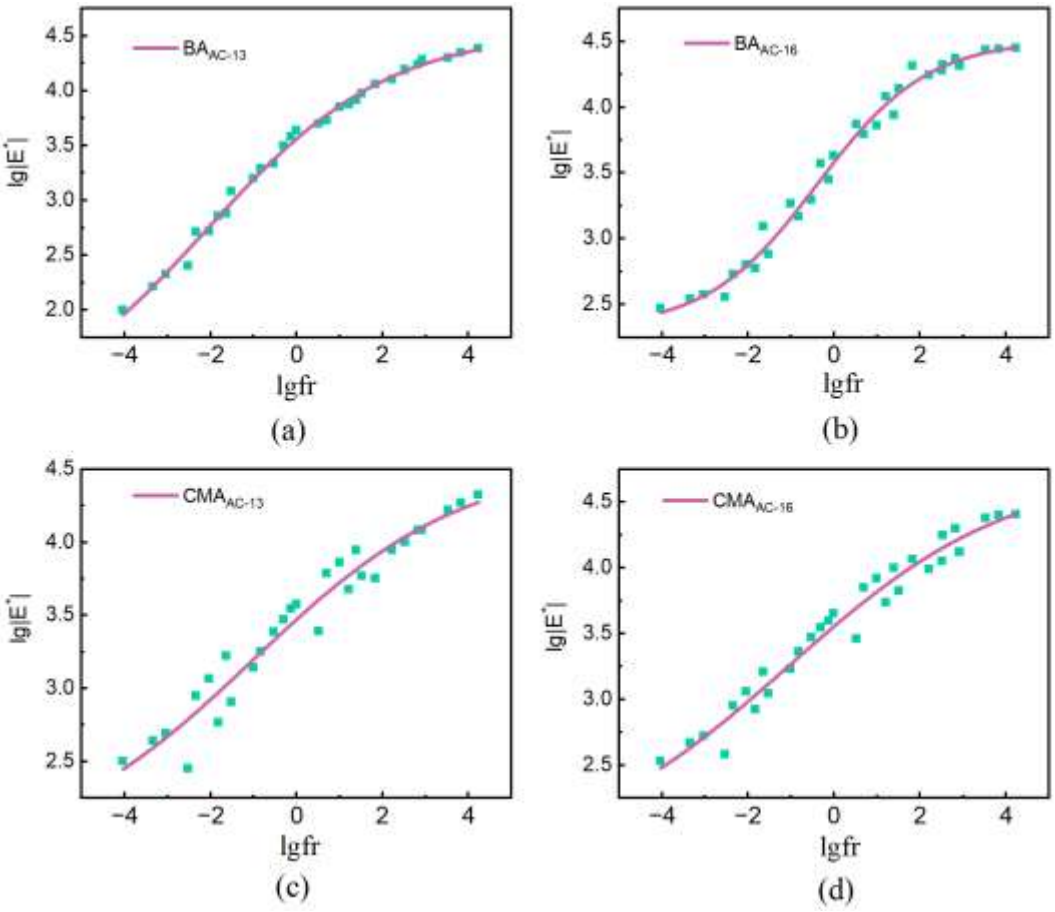

Figure 16. Master curve of E^*: **(a)** BA_{AC-13}; **(b)** BA_{AC-16}; **(c)** CMA_{AC-13}; **(d)** CMA_{AC-16}.

 doi:10.20944/preprints202502.0577.v1

4.Conclusions

This paper investigates the viscoelastic evolution of CMA materials through microscopic analysis, rheological testing, and the viscoelastic analysis of mixtures, leading to the following key conclusions:

(1) In terms of molecular structure, the findings indicate that the incorporation of SBS and SBR increases the levels of carbonyl and sulfoxide factors while reducing the level of long-chain factors, which slows the rate of change in large molecule content and enhances the aging resistance of the asphalt. Regarding molecular weight components, the addition of SBS and SBR reduces the rate of change of LMS by over 6%, while also mitigating the rate of change in overall molecular weight distribution to below 50%.

(2) Under dynamic loading conditions, the simultaneous incorporation of SBS and SBR into CMA mixtures increases the dynamic modulus in the 25Hz and -10 ℃ range by 24.3%(AC-13), 15.4%(AC-16), and reduces the φ by 55.8%(AC-13), 40%(AC-16).

(3) This study clarifies the evolution patterns of the characteristic functional groups and molecular weight of CMA. However, there remain limitations in revealing the viscoelastic evolution of the binder from a compositional perspective. Future research could conduct a four-component analysis of CMA, quantitatively characterizing the contents of asphaltenes, aromatics, saturated fractions, and resins to evaluate the impact of compositional changes on the viscoelastic properties of CMA.

Funding: This research was Sponsored by Natural Science Foundation of Xinjiang Uygur Autonomous Region(2023D01B26).

Institutional Review Board Statement: Not applicable

Conflicts of Interest: No conflicts of interest.

References

1. Chen H, Rabbira Garba Saba, Liu G, et al. Influence of material factors on the determination of dynamic moduli and associated prediction models for different types of asphalt mixtures. *Constr. Build. Mater*. **2023**, 365: 130-134.
2. Xiang L, Cheng J, Kang S, et al. Thermal oxidative aging mechanism of crumb rubber/SBS composite modified asphalt. *Constr. Build. Mater*. **2015**, 75:169-175. DOI: 10.1016/j.conbuildmat.2014.08.035.
3. Soon, Lee J, Serji N, et al. Short-term aging characterization of asphalt binders using gel permeation chromatography and selected Superpave binder tests. *Constr. Build. Mater*. **2008**, 22(11):2220-2227. DOI: 10.1016/j.conbuildmat.2007.08.005.
4. Zhang H , Chen Z , Xu G ,et al. Physical, rheological and chemical characterization of aging behaviors of thermochromic asphalt binder. *Fuel*. **2018**, 211(jan.1):850-858. DOI: 10.1016/j.fuel.2017.09.111.
5. Yao X, Wang Y, Xu T. Development on recycling, aging simulation and regeneration methods of reclaimed styrene-butadiene-styrene modified asphalt. *J. Clean. Prod.* **2021**, 312(1):127767. DOI: 10.1016/j.jclepro.2021.127767.
6. Zhang, J., Guo, N.S., Cui, S. C, et al. Preparation and performance analysis of polyamide-based rapid repair material for asphalt pavement shallow groove. *Constr. Build. Mater*. **2024**,419. doi.org/10.1016/j.conbuildmat.2024.135416
7. Menapace I, Masad E. Evolution of the microstructure of unmodified and polymer modified asphalt binders with aging in an accelerated weathering tester. *J. Microsc.* **2016**, 263(3): 341-356.DOI:10.1111/jmi.12405.
8. Liu Y , Xu X , Huang Z ,et al. Discrete-continuous coupling simulation and analysis for asphalt pavement dynamic stress responses under a moving wheel load. *Case. Stud. Constr. Mater*. **2023**, 18.DOI: 10.1016/j.cscm.2023. e01932.
9. Xu S, Tang G, Pan S, et al. Application of reactive rejuvenator in aged SBS modified asphalt regeneration: A review. *Constr. Build. Mater*. **2024**, 421. DOI: 10.1016/j.conbuildmat.2024.135696.

 doi:10.20944/preprints202502.0577.v1

10. Han D, Hu G, Zhang J. Study on Anti-Aging Performance Enhancement of Polymer Modified Asphalt with High Linear SBS Content. *Polymers*. **2023**, 15(2). DOI: 10.3390/polym15020256.
11. Xiao X , Wang J , Wang T ,et al. Linear viscoelasticity of asphalt in view of proportion and polarity of SARA fractions. *Fuel*. **2024**, 363. DOI: 10.1016/j.fuel.2024.130955.
12. Yu Z, Ban X, Xu Y, et al. Study on the Rheological Performance and Microscopic Mechanism of PPA/SBS/SBR Composite-Modified Asphalt Cold Replenishment Liquid. *Appl. Sci.* **2023**, 13(20), 11193; DOI. 3390/app132011193.
13. Ruan Y, Davison R R, Glover C J. The effect of long-term oxidation on the rheological properties of polymer modified asphalts. *Fuel*. **2003**, 82(14):1763-1773. DOI: 10.1016/S0016-2361(03)00144-3.
14. Wu, S., Pang, L., Liu, G. & Zhu, J., 2010. Laboratory study on ultraviolet radiation aging of bitumen. *J. Mater. Civil. Eng*. **2010**,22 (8), 767-772. DOI:10.1061/(asce)mt.1943-5533.
15. Chen Z , Zhang H , Shi C ,et al. Rheological performance investigation and sustainability evaluation of asphalt binder with thermochromic powders under solar radiation. *Sol. Energ. Mat. Sol. C.* **2019**, 191:175-182. DOI: 10.1016/j.solmat.2018.11.017.
16. GUO M., YIN X., DU X., et al., Effect of Aging, Testing Temperature and Relative Humidity on Adhesion between Asphalt Binder and Mineral Aggregate. *Constr. Build. Mater*. **2023**, 363(11): 129775. DOI:10.2139/ssrn.4214204
17. YANG B., LI H., XIE N., et al., Surface Characteristics of Ageing Asphalt Binder Coupling Thermal Oxidation and Ultraviolet Radiation. *Transport. Res. Rec.* **2022**, 2676(10): DOI: 147-162. doi.org/10.1177/03611981221088583
18. Yang B , Li H , Zhang H ,et al. Laboratorial investigation on effects of microscopic void characteristics on properties of porous asphalt mixture. *Constr. Build. Mater*. **2019**, 213:434-446. DOI: 10.1016/j.conbuildmat.2019.04.039.
19. Remisova E, Briliak D. Evaluation of the Effect of Thermo-Oxidative Aging and UV Radiation on Asphalt Stiffness. *Materials*. **2023**, 16.DOI:10.3390/ma16103716.
20. ZHAO Z., XU L., DU Z., et al., Moisture resistance of stone matrix asphalt at lab simulated high temperature and continuous rainfall condition. *Int. J. Pavement Eng.* **2022**, 1-12. DOI:10.1080/10298436.2022.2096884.
21. Feng B, Wang H, Li S, et al. The durability of asphalt mixture with the action of salt erosion: A review. *Constr. Build. Mater*. **2022**(Jan.10):315.
22. Zhang K, Li W, Han F. Performance deterioration mechanism and improvement techniques of asphalt mixture in salty and humid environment. *Constr. Build. Mater*. **2019**, 208: 749-757. DOI: 10.1016/j.conbuildmat.2019.03.061.
23. B H J A, C M M K, B H N, et al. Sustainable asphalt concrete containing high reclaimed asphalt pavements and recycling agents: Performance assessment, cost analysis, and environmental impact. *J. Clean. Prod.* **2019**, 244. DOI: 10.1016/j.jclepro.2019.118837.
24. Jattak Z A, Hassan N, Satar M. Moisture Susceptibility and Environmental Impact of Warm Mix Asphalt Containing Bottom Ash. *Case. Stud. Constr. Mater*. 2021, 15.DOI:10.1016/J.CSCM.2021.E00636.
25. Ling M, Luo X, Gu F, et al. Time-temperature-aging-depth shift functions for dynamic modulus master curves of asphalt mixtures. *Constr. Build. Mater*. **2017**, 157:943-951. DOI: 10.1016/j.conbuildmat.2017.09.156.
26. Shuai Zhang, Henglong Zhang, Mingyu Zhou, Investigation on the high-temperature stability and fatigue behavior of cold mixed epoxy asphalt mixture with different gradations *Case. Stud. Constr. Mater*.**2024**,20. DOI: 10.1016/j.cscm.2023. e02694
27. SIRIN O., PAUL D.K., KHAN M.S., et al., Effect of Aging on Viscoelastic Properties of Asphalt Mixtures. *J. Transp. Eng. B-Pave*. **2019**, 145(4): 04019034.DOI:10.1061/jpeodx.0000137
28. Al-Tawalbeh A, Sirin O, Sadeq M, et al. Evaluation and calibration of dynamic modulus prediction models of asphalt mixtures for hot climates: Qatar as a case study. *Case. Stud. Constr. Mater*. **2022**. DOI: 10.1016/j.cscm.2022. e01580.
29. Nobakht M, Sakhaeifar M S. Dynamic modulus and phase angle prediction of laboratory aged asphalt mixtures. *Constr. Build. Mater*. **2018**, 190:740-751. DOI: 10.1016/j.conbuildmat.2018.09.160.

30. Peyman S, Amirhossein K, Shadan T, et al. A comprehensive evaluation of damping, vibration, and dynamic modulus in reclaimed asphalt pavement: The role of rejuvenators, polymer, temperature, and aging. *Case. Stud. Constr. Mater*. **2024**,21, DOI: 10.1016/j.cscm.2024,
31. JI Y., CAO L., LI Z., et al., Numerical Conversion Method for the Dynamic Storage Modulus and Relaxation Modulus of Hydroxy-Terminated Polybutadiene (HTPB) Propellants. *Polymers*. **2022**, 15(3): 1-17. DOI:10.3390/polym15010003.
32. Bhattacharjee S, Swamy A K, Daniel J S. Continuous relaxation and retardation spectrum method for viscoelastic characterization of asphalt concrete. *Mech. Time. Depend. Mat.* **2012**, 16(3):287-305. DOI: 10.1007/s11043-011-9162-9.
33. Forough S A, Nejad F M, Khodaii A. Comparison of tensile and compressive relaxation modulus of asphalt mixes under various testing conditions. *Mater. Struct*. **2016**, 49(1-2):207-223. DOI: 10.1617/s11527-014-0489-y.
34. Liu H, Li Y, Fan G, et al. Uniform moduli characterization of asphalt mixtures under dynamic and static loading conditions. *Case. Stud. Constr. Mater*. **2023**, 19. DOI: 10.1016/j.cscm.2023. e02527.
35. Zhang H L , J. Y. Y U , Feng Z G ,et al. Effect of aging on the morphology of bitumen by atomic force microscopy. *J. Microsc. Oxford.* **2012**, 246(1):11-19. DOI: 10.1111/j.1365-2818.2011. 03578.x.
36. ZHAO Z., XIAO F., TORALDO E., et al., Effect of Crumb Rubber and Reclaimed Asphalt Pavement on Viscoelastic Property of Asphalt Mixture. *J. Clean. Prod.* **2023**, 428(20): 139422.
37. Wang H, Xueyan L, Apostolidis P, et al. Effect of laboratory aging on chemistry and rheology of crumb rubber modified bitumen. *Mater. Struct*. **2020**, 53(26). DOI: 10.1617/s11527-020-1451-9.
38. Petersen J C. A Review of the Fundamentals of Asphalt Oxidation: Chemical, Physicochemical, Physical Property, and Durability Relationships. *J. Traffic. Transp. Eng. (Engl. Ed.).* **2009**, E-C140. DOI: 10.17226/23002
39. Yongli Z, Fan G U, Jing X U, et al. Analysis of aging mechanism of SBS polymer modified asphalt based on Fourier transform infrared spectrum. *J. Wuhan. Univ. Technol*. **2010**(6):6. DOI:10.1007/s11595-010-0147-3.
40. Wang, P., Zhai, F., Dong, Z.J,et al. Micromorphology of Asphalt Modified by Polymer and Carbon Nanotubes through Molecular Dynamics Simulation and Experiments: Role of Strengthened Interfacial Interactions. *Energy. Fuels*. **2018**b,32 (2), 1179-1187
41. Wang R, Yue M, Xiong Y, et al. Experimental study on mechanism, aging, rheology and fatigue performance of carbon nanomaterial/SBS-modified asphalt binders. *Constr. Build. Mater*. **2020**, 268. DOI: 10.1016/j.conbuildmat.2020.121189.
42. Shen J, Amirkhanian S N, Lee S J. HP-GPC Characterization of Rejuvenated Aged CRM Binders. *J. Mater. Civ. Eng.* **2007**, 19(6):515-522. DOI:10.1061/(ASCE)0899-1561(2007)19:6(515).
43. Xu S, Huang R, Fang L, et al. Novel rejuvenators for sustainable recycling of aged SBS modified bitumen: Performance evaluation and reactive mechanism analysis. *J. Clean. Prod.* **2024**, 434. DOI:1 0.1016/j.jclepro.2023.140147.
44. Ma J , Sun G , Sun D ,et al. Application of gel permeation chromatography technology in asphalt materials: A review. *Constr. Build. Mater*. **2021**, 278. DOI: 10.1016/j.conbuildmat.2021.122386.